Inclusion of Electric Octupole Contributions Explains the Fast Radiative Decays of Two Metastable States in Ar^+

P. Lundin,[1] J. Gurell,[1] L.-O. Norlin,[2] P. Royen,[1] S. Mannervik,[1] P. Palmeri,[3] P. Quinet,[3,4] V. Fivet,[3] and É. Biémont[3,4]

[1]*Department of Physics, Stockholm University, AlbaNova University Center, SE-10691 Stockholm, Sweden*
[2]*Department of Physics, Royal Institute of Technology, AlbaNova University Center, SE-10691 Stockholm, Sweden*
[3]*Astrophysique et Spectroscopie, Université de Mons-Hainaut, B-7000 Mons, Belgium*
[4]*IPNAS, Université de Liège, Sart Tilman B15, B-4000 Liège, Belgium*

(Received 18 September 2007; published 20 November 2007)

A laser probing investigation has yielded the lifetimes of the $3s^2 3p^4(^1D)3d\ ^2G_{7/2,9/2}$ metastable doublet states of Ar^+. The results, obtained with the CRYRING ion storage ring of Stockholm, are 3.0 ± 0.4 and 2.1 ± 0.1 s, respectively. Comparisons with theoretical values calculated with two independent theoretical approaches, i.e., the pseudorelativistic Hartree-Fock method and the multiconfiguration Breit-Pauli approach, have allowed us to establish the unexpected and extraordinary strong contribution of an electric octupole ($E3$) transition to the ground state, in addition to the $M1$ decay channels to the $3d\ ^{2,4}F$ states and the $E2$ contributions to the $4s\ ^2P$, ^2D states.

DOI: 10.1103/PhysRevLett.99.213001 PACS numbers: 31.15.Ar, 32.30.−r, 32.70.Cs

Most singly charged atomic ions have metastable states that can live very long (lifetimes of the order of seconds or even more). Such levels usually decay to the ground state by magnetic dipole ($M1$) or electric quadrupole ($E2$) transitions (denoted 'forbidden transitions'). These second order transitions are generally 10^5–10^8 times weaker than allowed electric dipole ($E1$) transitions. As examples, the metastable ^2D_J levels in the singly-charged alkaline earth elements Ca^+, Sr^+ and Ba^+ have attracted much interest lately. The $5d\ ^2D_{3/2}$ level in Ba^+ has a lifetime of 89 s (see Ref. [1] and references therein) which is the longest lifetime that has been directly measured so far. Higher order transitions, i.e., magnetic quadrupole ($M2$) or electric octupole ($E3$) contributions to the decay channels, are generally still orders of magnitude weaker and in most cases negligible. To the best of our knowledge, the only reported electric octupole transition in a singly-charged ion is the $^2S_{1/2} - {}^2F_{7/2}$ in Yb^+, with an intensity corresponding to a radiative lifetime of 10 years [2,3], yielding an extremely narrow natural linewidth. The expansion coefficients for the high order terms have an increasingly high power dependence on the actual transition energies and, consequently, the high order contributions will be more important as the transition energy increases. This is the case for highly charged ions, for which the transitions may appear in the x-ray region and many high order transitions are observed. This is the reason that Beiersdorfer *et al.* [4] could observe as high order as a magnetic octupole ($M3$) transition at 2.7 keV in U^{64+}.

Singly charged ions of noble gases are special since the excitation energies are extraordinarily high. While the $^2D_{3/2}$ level in Ba^+, mentioned above, has an excitation energy of 0.6 eV, the lowest excitation energies in Ar^+, Kr^+ and Xe^+ are 20 times higher or more. Lifetimes of metastable levels have been determined by the laser probing technique [5,6] (LPT) developed at the ion storage ring CRYRING at the Manne Siegbahn Laboratory. We have published results in Xe^+ observing a hyperfine effect for a very long-lived level [7] and measuring lifetimes of some more short-lived levels (ms lifetimes) [8]. Later on results for Ar^+ were presented [9]. For measurements in Kr^+ we originally found a significant discrepancy between our experimental and theoretical results. Finally we could rule out that this could be due to experimental problems and therefore we decided to include higher order effects in the calculations and unexpectedly it turned out that the level's decay was dominated by a magnetic quadrupole decay ($M2$) [10]. This intriguing result inspired us to revisit the long-lived $5d\ ^4D_{7/2}$ level in Xe^+. Also here calculations showed that this decay was dominated by a third order effect, namely, a magnetic quadrupole transition. Because of the magnetic field sensitivity of this particular state the experiment was more demanding, but finally the magnetic field effect could be disentangled and the experimental results confirmed the theoretical findings [11]. Our previous study of Ar^+ [9] presented mainly calculations of lifetimes in which second order contributions ($M1$ and $E2$) were included. At this time we had not yet realized the importance of higher order contributions. The experimental part was more restricted in that work and the weak signals permitted only one lifetime to be experimentally determined. With the new results in Kr^+ and Xe^+ in mind we decided to study Ar^+ once more.

In the present study, we were interested in the decay properties of the $3s^2 3p^4(^1D)3d\ ^2G_{7/2,9/2}$ levels in Ar^+. These metastable states can decay to lower energy levels of the same configuration and of the $3s^2 3p^4 4s$ configuration via magnetic dipole ($M1$) and electric quadrupole ($E2$) transitions (see Fig. 1). More interestingly, they can also be connected to the ground term $3s^2 3p^5\ ^2P^o$ through higher

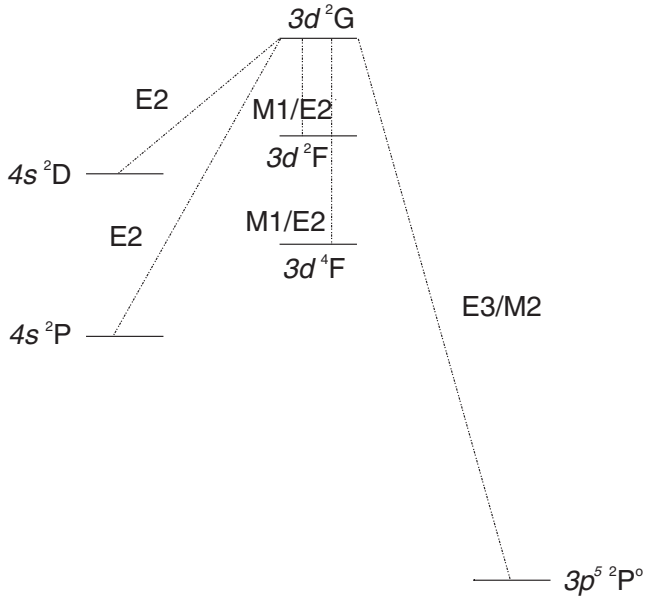

FIG. 1. Schematic partial Grotrian diagram of Ar^+. Only the main decay channels of the $3s^2 3p^4(^1D)3d\ ^2G$ term are indicated.

order transitions, primarily by electric octupole ($E3$) transitions. These transitions are expected to appear in the UV region (around 65 nm) and the transition probabilities are likely to be enhanced by a strong wavelength effect like the ones observed in Kr^+ [10] and Xe^+ [11]. Contrary to these last two cases however, the $M2$ decay channel is forbidden by the LS selection rules while the $E3$ transitions are allowed [3]. Allowing for departure from LS selection rules, the $3s^2 3p^4(^1D)3d\ ^2G_{7/2}$ may decay through $M2$ without breaking the selection rules for J ($\Delta J = 0, \pm 1$ or ± 2) while the other doublet with $J = 9/2$ cannot. This situation renders the $3s^2 3p^4(^1D)3d\ ^2G_{7/2,9/2}$ levels of Ar^+ particularly attractive for a detailed experimental and theoretical investigation of their radiative properties, which is now reported in this Letter.

Argon gas was injected into the ion source of Nielsen-type, where the atoms were ionized due to collisions with electrons. The ions were extracted and then accelerated to 40 keV, isotope separated in a 90° bending magnet where $^{40}Ar^+$ was selected and finally transported and injected into the storage ring. The ion beam current during the experiment was typically 5 μA and the pressure inside the ring was below 10^{-11} Torr. During the ion production a small fraction of the ions were populating the metastable level of interest. The stored ion beam will decay due to collisions between ions and residual gas inside the ring. This decay of the ion beam was monitored with a multichannel plate (MCP) [12] neutral particle detector, mounted after one of the bending magnets, connected to a multiscaler. The MCP was also used to monitor the amount of ions injected every ring cycle.

The lifetime was measured by the LPT, described in detail previously [5,6]. The populations of the $3d\ ^2G_{7/2}$ and $3d\ ^2G_{9/2}$ levels were probed through a laser induced excitation to a short-lived higher lying level, $3s^2 3p^4(^1D)4p\ ^2F^o_{7/2}$, with a lifetime of $\tau = 8.41 \pm 0.03$ ns [13]. The intensity of the fluorescence from this upper level, detected by a photomultiplier, is proportional to the population of the metastable level. By applying laser probe pulses at different delay times relative to ion injection into the storage ring the lifetime curve of the metastable level was recorded.

Some systematic effects have to be corrected for in the experiment, e.g., repopulation (collisional excitation) and collisional deexcitation. The repopulation will increase the population of the metastable level through collisions between stored ions and rest gas inside the storage ring, an effect which will make the measured and observed lifetime appear longer. A technique has been developed to record this effect in order to correct for it [5,14]. Collisional deexcitation will, in contrast to the repopulation, deplete the metastable state and shorten the observed lifetime. This effect was corrected for by measuring the lifetime at different pressures inside the ring. The measured decay rate is then plotted as a function of pressure in a Stern-Vollmer plot from which the radiative decay rate was extracted at zero pressure, see Fig. 2. The contribution to the lifetime curve from repopulation was in this experiment small and only caused a 1% correction to the observed lifetime. A number of normalization curves are regularly recorded in order to correct for possible variations in the ion beam intensity, metastable state population and laser beam stability. In the present experiment these corrections were negligible.

The extracted lifetimes for the metastable levels $3d\ ^2G_{7/2}$ and $3d\ ^2G_{9/2}$ in Ar^+ were experimentally determined to be 3.0 ± 0.4 s and 2.1 ± 0.1 s. The uncertainty listed with each value is the standard deviation from the fitted curve where the main part comes from statistical

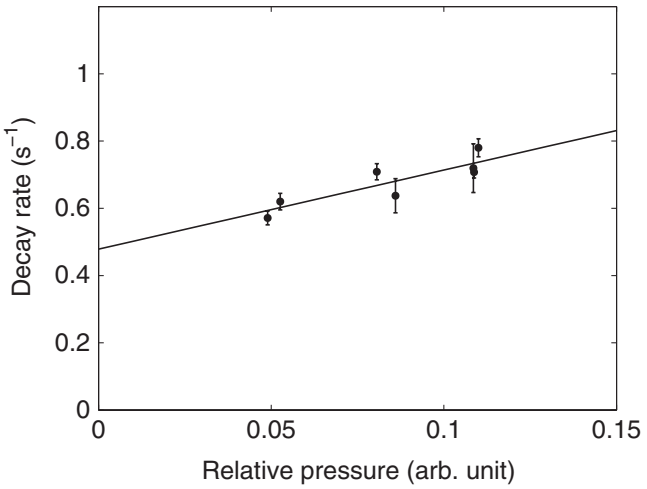

FIG. 2. Stern-Vollmer plot for the $3d\ ^2G_{9/2}$ level.

spread between the measured pressure points, as well as from subtraction of repopulation.

In order to compute the radiative parameters of the transitions depopulating the $3s^23p^4(^1D)3d\ ^2G_{7/2,9/2}$ metastable states, we considered two independent structures: i.e., the Hartree-Fock pseudorelativistic (HFR) method implemented in Cowan's chain of computer codes [15] and the multiconfiguration Breit-Pauli (MCBP) approach implemented in the AUTOSTRUCTURE code [16].

In the HFR approach, configuration interaction (CI) was retained among 38 configurations, i.e., those considered previously by Schef *et al.* [9] to which we have added the $3s^23p^33d4p$, $3s^23p^34s4p$, $3s3p^43d4s$, $3s^23p^23d^3$, $3s^23p^23d^24s$, and $3s^23p^23d4s^2$ configurations. Using the experimental energies compiled at NIST [17], the HFR method was then combined with a least-squares optimization routine minimizing the discrepancies between the experimental and calculated energy levels belonging to the $3s3p^6$, $3s^23p^43d$ and $3s^23p^44s$ configurations. The Slater integrals (F^k, G^k and R^k) corresponding to the remaining configurations were scaled down by a factor 0.85 according to a well established procedure [15].

In the MCBP calculation, single electron orbitals, $P_{\rm nl}(r)$, were constructed by diagonalizing the nonrelativistic Hamiltonian using a scaled statistical Thomas-Fermi-Dirac model potential $V(\lambda_{\rm nl})$ [18]. The $\lambda_{\rm nl}$ scaling parameters were optimized variationally by minimizing a weighted sum of the LS term energies. LS terms are represented by CI wave functions of the type

$$\Psi = \sum_i c_i \Phi_i. \tag{1}$$

Relativistic fine-structure levels and transition rates are obtained by diagonalizing the Breit-Pauli Hamiltonian in intermediate coupling. The one- and two-body fine-structure and non-fine-structure operators have been fully implemented to the order $\alpha^2 Z^4$, where α is the fine-structure constant and Z the atomic number. Semiempirical corrections take the form of term energy corrections (TEC). By considering the relativistic wave functions, Ψ_i^r, in a perturbation expansion of the nonrelativistic wave functions, $\Psi_i^{\rm nr}$, we have

$$\Psi_i^r = \Psi_i^{\rm nr} + \sum_{j\neq 1} \Psi_i^{\rm nr} \frac{\langle \Psi_j^{\rm nr} | H_{1b} + H_{2b} | \Psi_i^{\rm nr} \rangle}{E_i^{\rm nr} - E_j^{\rm nr}}, \tag{2}$$

where H_{1b} and H_{2b} are, respectively, the one-body and two-body parts of both fine-structure and non-fine-structure Hamiltonians. A modified nonrelativistic Hamiltonian is constructed with improved estimates of the differences $E_i^{\rm nr} - E_j^{\rm nr}$ so as to adjust the centers of gravity of the spectroscopic terms to the available experimental values.

The CI expansion included the following configurations: $3s^23p^5 + 3s^23p^4np(n=4-5) + 3s^23p^4nf(n=4-5) + 3s3p^53d + 3s3p^54s + 3s3p^43d4p + 3s3p^44s4p + 3p^64p + 3p^53d^2 + 3p^53d4s + 3p^54s^2 + 3s^23p^33d^2 + 3s^23p^33d4s + 3s^23p^34s^2 + 3s^23p^34p^2$ in the odd parity, and $3s3p^6 + 3s^23p^4nd(n=3-5) + 3s^23p^4ns(n=4-5) + 3s^23p^45g + 3s3p^44s^2 + 3s3p^44p^2 + 3s3p^43d^2 + 3s3p^54p + 3p^63d + 3p^64s + 3s^23p^33d4p + 3s^23p^34s4p + 3s3p^43d4s + 3s^23p^23d^3 + 3s^23p^23d^24s + 3s^23p^23d4s^2$ in the even parity. The scaling parameters have been optimized by minimizing the sum of all the 860 LS term energies. The optimized values were the following: $\lambda_{1s} = 1.4662$; $\lambda_{2s} = 1.1167$; $\lambda_{2p} = 1.0640$; $\lambda_{3s} = 1.1250$; $\lambda_{3p} = 1.1252$; $\lambda_{3d} = 1.1812$; $\lambda_{4s} = 1.1945$; $\lambda_{4p} = 1.1606$; $\lambda_{4d} = 1.1146$; $\lambda_{4f} = 1.1492$; $\lambda_{5s} = 1.1158$; $\lambda_{5p} = 1.0899$; $\lambda_{5d} = 1.1172$; $\lambda_{5f} = 1.1527$ and $\lambda_{5g} = 1.1518$. TEC have been applied to all the spectroscopic terms below 170 000 $\rm cm^{-1}$ as compiled in the NIST database [17].

In Table I, we compare the experimental lifetimes (τ in s) of the $3s^23p^4(^1D)3d\ ^2G_{7/2,9/2}$ levels of Ar^+ as obtained in the present work with the two different HFR and MCBP calculations. A general good agreement between theory and experiment is observed for the two levels. In the table, we present also the contributions ($\sum A$ in $\rm s^{-1}$) of the different decay modes ($M1$, $E2$, $M2$ and $E3$) to the lifetimes computed by the two methods. The $M2$ and $E3$ numerical values have been obtained only in the MCBP approach (see the starred values in the table) because Cowan's code [15] does not allow the calculations of these higher order corrections.

It has been found that the additional configurations considered in our HFR model play an important role, the total contributions ($M1 + E2$) to the $^2G_{7/2}$ and $^2G_{9/2}$ lifetimes calculated by Schef *et al.* [9] (not shown in this table) being increased by about 36% and 40%, respectively. The present model is justified by the fact that the most important core-valence correlation, as pointed out in Ref. [19], is

TABLE I. Contributions of the different decay modes to the lifetimes of the $3s^23p^4(^1D)3d\ ^2G_{7/2,9/2}$ levels computed by two independent methods (HFR and MCBP) and comparison with experiment.

Level	Type	$\sum A$ ($\rm s^{-1}$)[a]		
		HFR	MCBP	Experiment
$3s^23p^4(^1D)3d\ ^2G_{7/2}$	$M1$	1.96(−1)	2.46(−1)	···
	$E2$	2.63(−2)	2.67(−2)	···
	$M2$	1.51(−2)⋆	1.51(−2)	···
	$E3$	1.33(−1)⋆	1.33(−1)	···
	τ (s)	2.70	2.38	3.0 ± 0.4
$3s^23p^4(^1D)3d\ ^2G_{9/2}$	$M1$	2.77(−1)	3.44(−1)	···
	$E2$	8.45(−3)	1.42(−2)	···
	$E3$	1.35(−1)⋆	1.35(−1)	···
	τ (s)	2.38	2.03	2.1 ± 0.1

[a]HFR, MCBP, Experiment: this work. The a(b) notation stands for $a \times 10^b$. Starred values: from MCBP; see text.

included and also by the fact that it was shown in Ref. [9] that the contributions to the $M1$ and $E2$ decay rates of higher ($n > 8$) terms along the Rydberg series were negligible.

Table I shows the importance of the $E3$ transitions in the decay of both levels. They contribute up to 30% to the total decay. The agreement between the HFR and MCBP $M1$ and $E2$ contributions is within 20% and 40%, respectively. It should be emphasized that the $E3$ contributions are the fastest $E3$ transitions (of the order of a tenth of a s^{-1}) ever observed in an experiment.

It is interesting to compare the $E3$ rates for these transitions in Ar^+ with the only previously reported $E3$ transition in a singly charged ion. The calculated transition probability [3] for the $^2S_{1/2} - {}^2F_{7/2}$ transition in Yb^+ is 3.8×10^{-9} s^{-1}, a value that is consistent with the experimental estimate of a lifetime of 10 years [2] for the upper level. The Yb^+ transition appears at 467 nm, while the Ar^+ transitions discussed here are at 65 nm (observation not yet reported). Since the $E3$ transition rate depends on the transition energy to the seventh power the difference in wavelength will enhance the transition rate drastically. But if we correct for this energy factor, the Ar^+ rate is still about 36 times larger than for Yb^+ meaning that the matrix element is about 6 times larger. This relation is also obtained directly from the calculations using the Cowan code which yields the reduced matrix element for the $E3$ transition in Ar^+ to be $\langle 3p||\mathbf{r}^3||3d\rangle = 13.49$ a.u., while the corresponding matrix element for Yb^+ is $\langle 4f||\mathbf{r}^3||6s\rangle = -2.15$ a.u. [2]. This difference is essentially due to the principal and orbital quantum number changes of the jumping electron involved in the transition, i.e. $\Delta n = 0$, $\Delta l = 1$ for Ar^+ and $\Delta n = 2$, $\Delta l = 3$ for Yb^+.

We also note that for the $ns^2np^4(^3P)nd\,{}^4D_{7/2} - ns^2np^5\,{}^2P_{1/2,3/2}$ $E3$ transitions in Kr^+ ($n = 4$) [10] and in Xe^+ ($n = 5$) [11], the calculated rates were about 4 orders of magnitude smaller than the values obtained in the present work for Ar^+. Moreover, in contrast to Ar^+, the $E3$ contributions for Kr^+ and Xe^+ were negligible compared to the $M2$ ones. We conclude that the importance and amplitude of the $E3$ decay mode for the Ar^+ states reported here is quite extraordinary.

This work was supported by the Swedish Research Council (VR). The expertise of the CRYRING staff has been greatly appreciated. Financial support from the Belgian FR-FNRS (Fonds National de la Recherche Scientifique) and IISN (Institut Interuniversitaire des Sciences Nucléaires) is acknowledged. E. B. is Research Director of the FR-FNRS, P. P. and P. Q. are Research Associates of this organization and V. F. has a FRIA grant.

[1] J. Gurell, É. Biémont, K. Blagoev, V. Fivet, P. Lundin, S. Mannervik, L.-O. Norlin, P. Quinet, D. Rostohar, P. Royen, and P. Schef, Phys. Rev. A **75**, 052506 (2007).
[2] M. Roberts, P. Taylor, G. P. Barwood, P. Gill, H. Klein, and W. R. C. Rowley, Phys. Rev. Lett. **78**, 1876 (1997).
[3] É. Biémont and P. Quinet, Phys. Rev. Lett. **81**, 3345 (1998).
[4] P. Beiersdorfer, A. L. Osterheld, J. Scofield, B. Wargelin, and R. E. Marrs, Phys. Rev. Lett. **67**, 2272 (1991).
[5] S. Mannervik, Phys. Scr. **T105**, 67 (2003).
[6] J. Lidberg, A. Al-Khalili, L.-O. Norlin, P. Royen, X. Tordoir, and S. Mannervik, Nucl. Instrum. Methods Phys. Res., Sect. B **152**, 157 (1999).
[7] S. Mannervik, L. Broström, J. Lidberg, L.-O. Norlin, and P. Royen, Phys. Rev. Lett. **76**, 3675 (1996).
[8] J. Lidberg, A. Al-Khalili, R. D. Cowan, L.-O. Norlin, P. Royen, and S. Mannervik, Phys. Rev. A **56**, 2692 (1997).
[9] P. Schef, A. Derkatch, P. Lundin, S. Mannervik, L.-O. Norlin, D. Rostohar, P. Royen, and É. Biémont, Eur. Phys. J. D **29**, 195 (2004).
[10] É. Biémont, A. Derkatch, P. Lundin, S. Mannervik, L.-O. Norlin, D. Rostohar, P. Royen, P. Palmeri, and P. Schef, Phys. Rev. Lett. **93**, 063003 (2004).
[11] P. Schef, P. Lundin, É. Biémont, A. Källberg, L.-O. Norlin, P. Palmeri, P. Royen, A. Simonsson, and S. Mannervik, Phys. Rev. A **72**, 020501(R) (2005).
[12] A. Paal, 6th European Workshop on Beam Diagnostic and Instrumentation for Particle Accelerators (DIPAC, Mainz, Germany, 2003).
[13] D. Marger and H. Schmoranzer, Phys. Lett. **146**, 502 (1990).
[14] S. Mannervik, J. Lidberg, L.-O. Norlin, and P. Royen, Phys. Rev. A **56**, R1075 (1997).
[15] R. D. Cowan, *The Theory of Atomic Structure and Spectra* (University California Press, Berkeley, 1981).
[16] N. R. Badnell, J. Phys. B **19**, 3827 (1986); J. Phys. B **30**, 1 (1997).
[17] Y. Ralchenko, F.-C. Jou, D. E. Kelleher, A. E. Kramida, A. Musgrove, J. Reader, W. L. Wiese, and K. Olsen, NIST Atomic Spectra Database (version 3.1.2), http://physics.nist.gov/asd3 (2007).
[18] W. Eissner and H. Nussbaumer, J. Phys. B **2**, 1028 (1969).
[19] P. Quinet and J. E. Hansen, J. Phys. B **28**, L213 (1995).